SCIENTIFIC REPORTS

OPEN

Shape-controlled synthesis and influence of W doping and oxygen nonstoichiometry on the phase transition of VO_2

Received: 01 May 2015
Accepted: 18 August 2015
Published: 16 September 2015

Ru Chen[1,2], Lei Miao[1,3], Chengyan Liu[3], Jianhua Zhou[3], Haoliang Cheng[1], Toru Asaka[4], Yuji Iwamoto[4] & Sakae Tanemura[1,3]

Monoclinic VO_2(M) in nanostructure is a prototype material for interpreting correlation effects in solids with fully reversible phase transition and for the advanced applications to smart devices. Here, we report a facile one-step hydrothermal method for the controlled growth of single crystalline VO_2(M/R) nanorods. Through tuning the hydrothermal temperature, duration of the hydrothermal time and W-doped level, single crystalline VO_2(M/R) nanorods with controlled aspect ratio can be synthesized in large quantities, and the crucial parameter for the shape-controlled synthesis is the W-doped content. The dopant greatly promotes the preferential growth of (110) to form pure phase VO_2(R) nanorods with high aspect ratio for the W-doped level = 2.0 at% sample. The shape-controlled process of VO_2(M/R) nanorods upon W-doping are systematically studied. Moreover, the phase transition temperature (T_c) of VO_2 depending on oxygen nonstoichiometry is investigated in detail.

Vanadium dioxide (VO_2) plays a crucial role in many fundamental research and practical applications. For instance, Mott field-effect transistor, light modulator and optical storage medium are potential products based on VO_2[1–3]. Moreover, VO_2 with a metal-insulator phase transition (MIT) is a key material for applying to thermochromic smart windows because it exhibits a reversible structural transformation from an infrared-transparent monoclinic phase ($VO_2(M_1)$) at low temperature to an infrared-reflective rutile state (VO_2(R)) at higher temperature than the transition, while maintaining certain visible transmittance[4–7]. Whereas, VO_2 exhibits hysteresis in its phase transition properties and mechanical degradation on passing through the MIT because of stresses during the structural change[8]. In addition, the phase transition temperature (T_c) of MIT (68 °C) is always too high for the practical application of VO_2-based materials[4].

Nano-materials often exhibit extraordinary physical and chemical properties compared to their bulk counterparts[9]. One dimensional nanostructures, for example, nanorods represent particularly attractive because they present novel characteristics owing to their small radial dimension while retaining longitudinally connected substance[10]. In confined nanoscale system, more localized electronic states as well as narrower bands are usually supposed to increase the densities of states and lead to the superior phase transition behavior of VO_2[11]. Using the hydration-cleavage-exfoliation solvothermal process, Banerjee and co-workers have reduced the T_c of undoped VO_2 by synthesizing various sized nanostructures[12]. In their research, the phase transition temperature during the cooling cycle is more significantly affected than the heating cycle by nanostructuring, therefore, the hysteresis width is observed to be much wider

[1]Key Laboratory of Renewable Energy, Guangzhou Institute of Energy Conversion, Chinese Academy of Sciences, Guangzhou 510640, P. R. China. [2]University of Chinese Academy of Sciences, Beijing 100049, P. R. China. [3]Guangxi Key Laboratory of Information Material, Guangxi Collaborative Innovation Center of Structure and Property for New Energy and Materials, School of Material Science and Engineering, Guilin University of Electronic Technology, Guilin, 541004, P. R. China. [4]Department of Frontier Materials, Graduate School of Engineering, Nagoya Institute of Technology, Gokiso-cho, Showa-ku, Nagoya, 466-8555, Japan. Correspondence and requests for materials should be addressed to L.M. (email: miaolei@ms.giec.ac.cn)

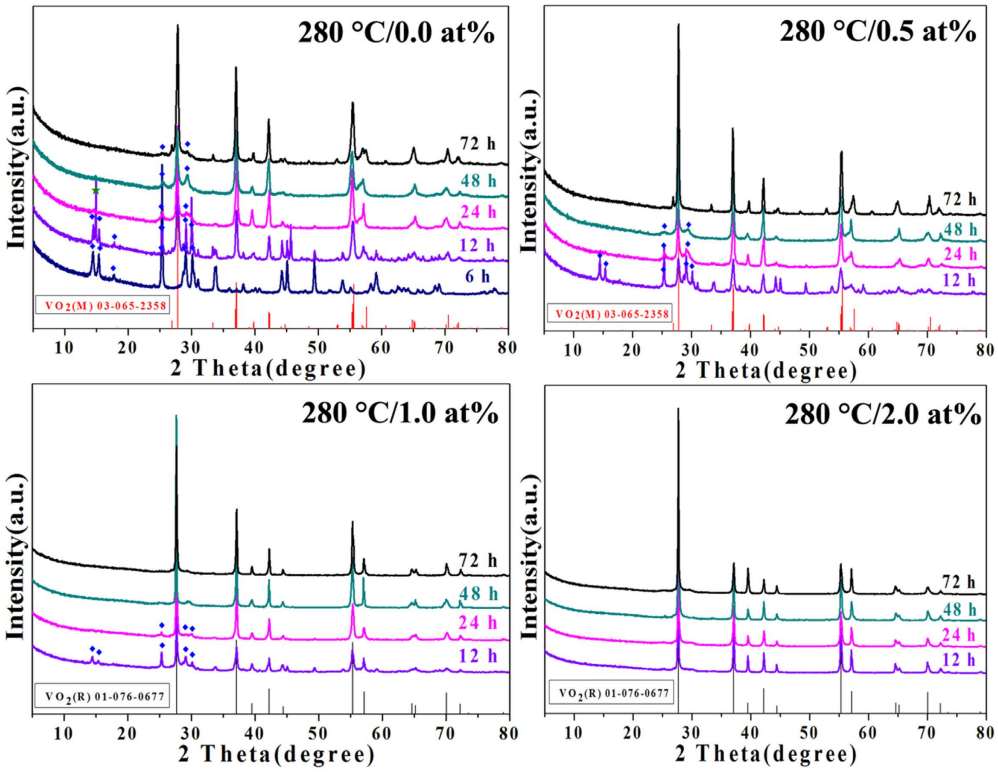

Figure 1. XRD patterns of $W_xV_{1-x}O_2$ prepared at 280 °C with W doping levels ranging from 0.0 to 2.0 at% for different duration of hydrothermal time. The filled dark blue diamond and olive star are characteristic peaks for B and A phase of VO_2 respectively. The red and black columns belong to standard pattern in JCPDS card No. 65–2358 for VO_2(M) and No. 76–0677 for VO_2(R) respectively.

for all the nanostructures. Gao and co-workers have also regulated the hysteresis width through the nano-size effect[13], which provides a key that nanoscale VO_2(M_1/R) possesses the probability of tuning hysteresis width for obtaining a sharper, more reproducible phase transition. Up to now, more than 20 compounds of vanadium oxide (VO, V_2O_3, VO_2, V_6O_{13}, V_8O_{15}, V_2O_5 and so on[14]) and 10 polymorphs of VO_2 (B, A, T, M_1, M_2, R phase and so on[15]) had been reported. Only the VO_2(M/R) (the M_1 phase is referred to as the M phase of VO_2 in this study) experiences a fully reversible MIT at the vicinity of room temperature (RT). Moreover, low temperature synthetic method has usually generated VO_2(B) nanobelts and subsequently can be transformed to VO_2(M/R) by the post-heating treatment, but the nanostructure has been nearly destroyed[16–18]. So it should be a challenge to synthesize pure phase VO_2(M/R) with a shape controlled nanostructure.

The ongoing debate associated to the fundamental origin of the phase transition behavior in VO_2 involves electron-correlation-driven (Mott transition)[19,20], structure-driven (Peierls transition)[21,22], or the cooperation of both[23]. W doping is known as an effective route to regulate electron density in the conduction band for decreasing T_c by approx. 20–26 °C/at% W for the bulk and by 50–80 °C/at% W in nanostructures[24–27]. Synthesis of VO_2(M/R) by controlling both the shape of nanostructures and the amount of W dopant could be a good strategy to narrow the hysteresis width while reducing T_c for obtaining an excellent phase transition property of VO_2-based materials. Of note, systematically experimental investigation of nonstoichiometric effect in VO_2 has been insufficient. The phase transition behavior has been demonstrated to be also sensitive to vanadium or oxygen related vacancies, even a deviation in the oxygen stoichiometry by a few percent can cause the lattice structure change and result in several orders of magnitude difference in the resistivity transition or the phase transition temperature shift[28,29]. Therefore, studying on oxygen nonstoichiometry induced reduction of T_c will contribute to the general understanding of the intrinsic MIT mechanism in VO_2.

In this study, we successfully explored a one-pot hydrothermal method to prepare VO_2(M/R) with desired morphology. It is inspiring to discover that the W dopant promotes the generation of pure phase VO_2(M/R) nanorods with high aspect ratio. Moreover, the effect of oxygen nonstoichiometry on the structural phase transition and subsequently T_c of VO_2 is discussed in detail.

Results

Shape-controlled synthesis and phase metamorphosis behavior upon W doping. Figure 1 shows the crystalline phase metamorphic behavior of $W_xV_{1-x}O_2$ with x = 0, 0.5, 1.0 and 2.0 at%

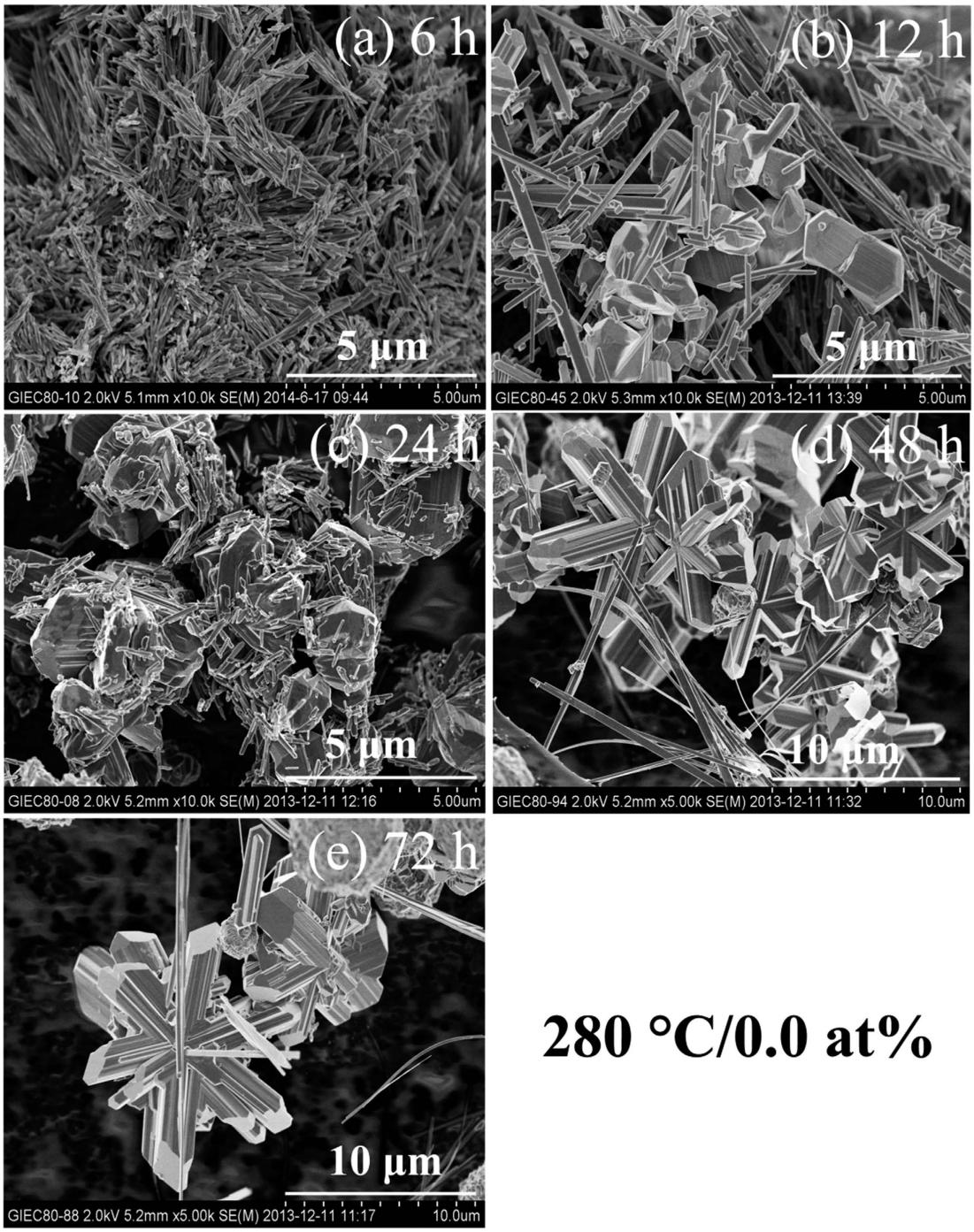

Figure 2. SEM images of undoped VO_2 synthesized at 280 °C for different duration of hydrothermal time.

respectively where the temperature being kept at 280 °C but the different duration of the hydrothermal time being applied. For the undoped VO_2, pure phase VO_2(B) is obtained for the duration of the hydrothermal time for 6 h. By increasing the duration of the hydrothermal time from 12 to 72 h, the peak of {011} for VO_2(M) (M {011} at around 27.8°) appears and becomes more significant. However, there always exists the secondary phase VO_2(B) in the final product. Serial SEM images in Fig. 2 show the morphology transition behavior of the undoped VO_2 upon increasing the duration of the hydrothermal time. Products of the metastable VO_2(B) are the tangled nanobelts in the morphology for the 6 h-sample. By increasing the duration of the hydrothermal time from 12 to 72 h, VO_2(B) nanobelts always exist as partial morphology except the block or snowflake VO_2(M). In conclusion, we could not synthesize pure phase VO_2(M) without W doping.

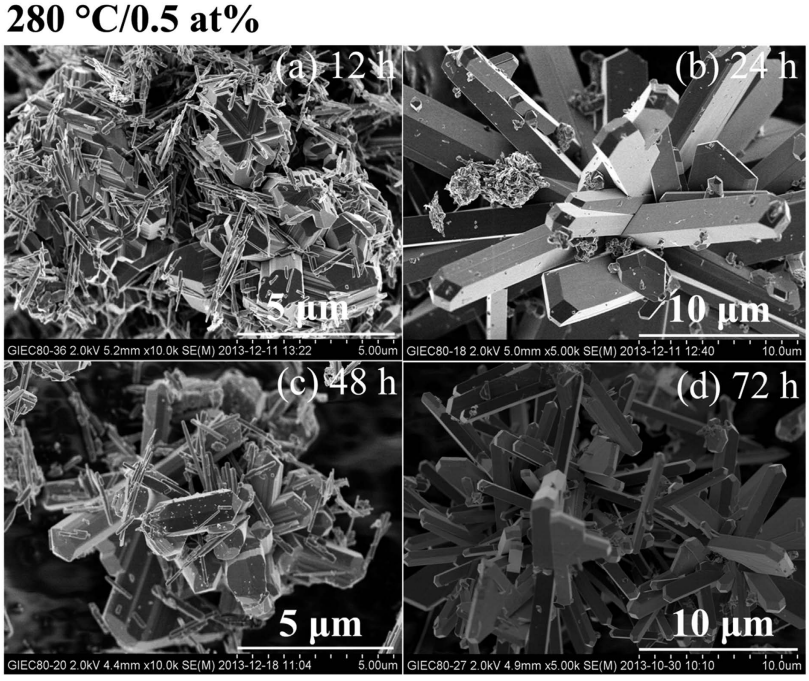

Figure 3. SEM images of $W_xV_{1-x}O_2$ (x = 0.5 at%) synthesized at 280 °C for different duration of hydrothermal time.

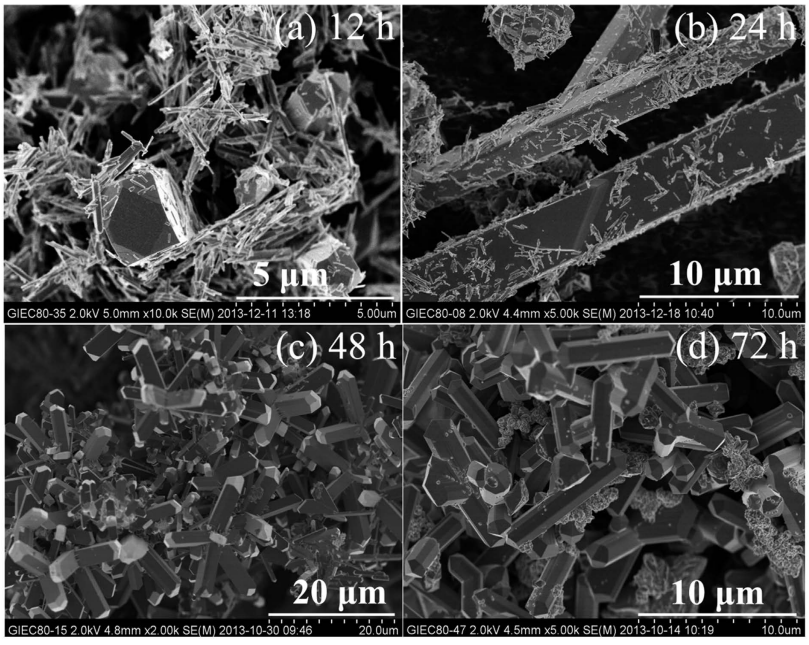

Figure 4. SEM images of $W_xV_{1-x}O_2$ (x = 1.0 at%) synthesized at 280 °C for different duration of hydrothermal time.

By increasing the W-doped level to 0.5 at%, VO_2(B) nanobelts always exist as partial morphology except the snowflake or rod-like VO_2(M) for the duration of the hydrothermal time $\leq$48 h as shown in Figs 1 and 3. Inspiringly, the peaks of VO_2(B) vanish and pure phase VO_2(M) ($T_c > RT$) with uniformly rod-like morphology is successfully synthesized for the 72 h-sample. Meanwhile, for the hydrothermal samples prepared at 280 °C with W-doped of 1.0 and 2.0 at%, pure phase VO_2(R) with uniformly rod-like morphology is obtained when the duration of the hydrothermal time $\geq$48 h and $\geq$12 h respectively as shown in Figs 1,4 and 5. The synchrotron radiation X-ray powder diffraction (SRXPD, $\lambda = 0.50$ Å)

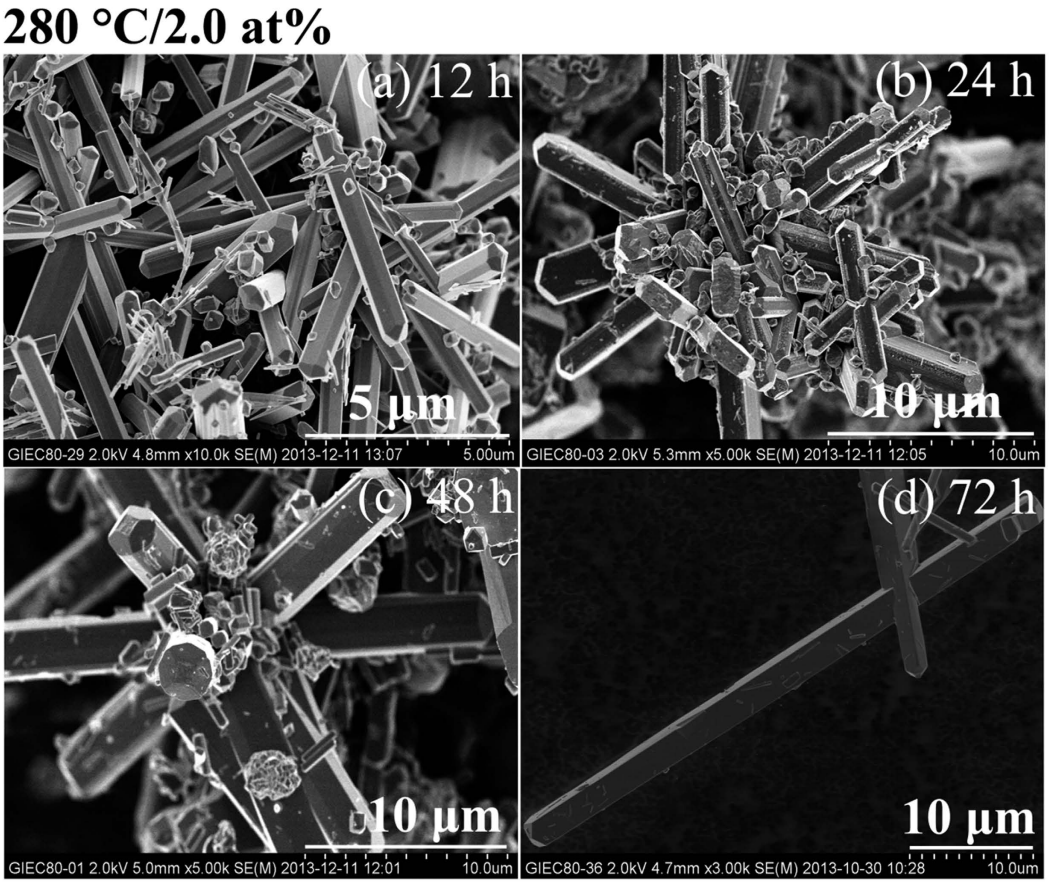

Figure 5. SEM images of $W_xV_{1-x}O_2$ (x = 2.0 at%) synthesized at 280 °C for different duration of hydrothermal time.

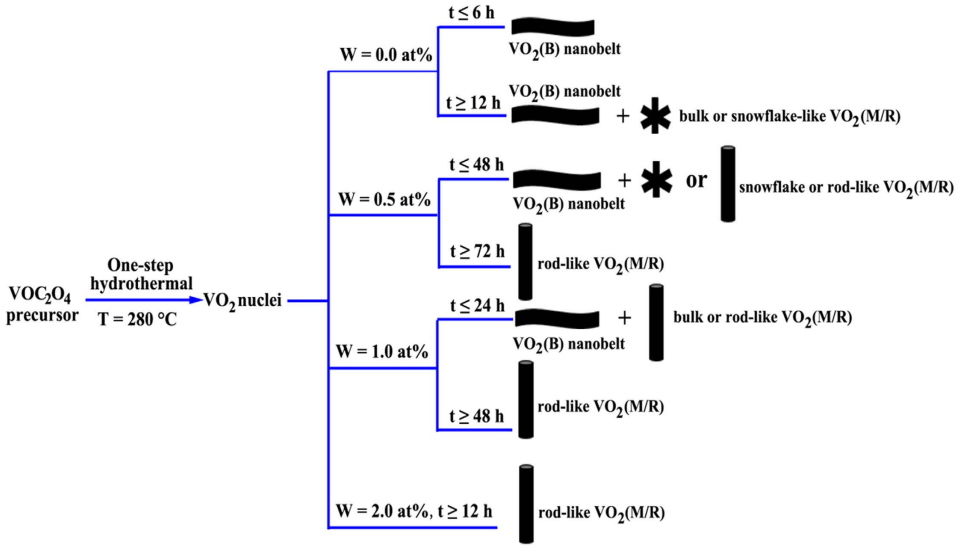

Figure 6. Schematic illustration of the morphology metamorphic behavior of VO_2.

data confirm the pure phase VO_2(M/R) is exactly free from the existing of the other V-O compounds and other VO_2 phases, which was reported by our group in the recently study[30]. As an overall comparison, the schematic illustration of the morphology metamorphic behavior of VO_2 is summarized in Fig. 6.

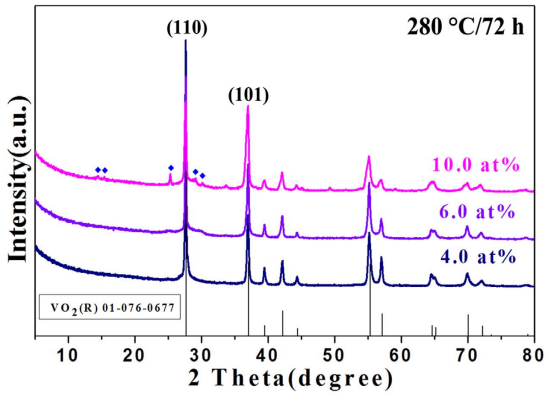

Figure 7. XRD patterns of the $W_xV_{1-x}O_2$ prepared at 280 °C for 72 h with W doping levels ranging from 4.0 to 10.0 at%. The filled dark blue diamond is characteristic peaks for B phase of VO_2. The black column belongs to standard pattern in JCPDS card No. 76–0677 for VO_2(R).

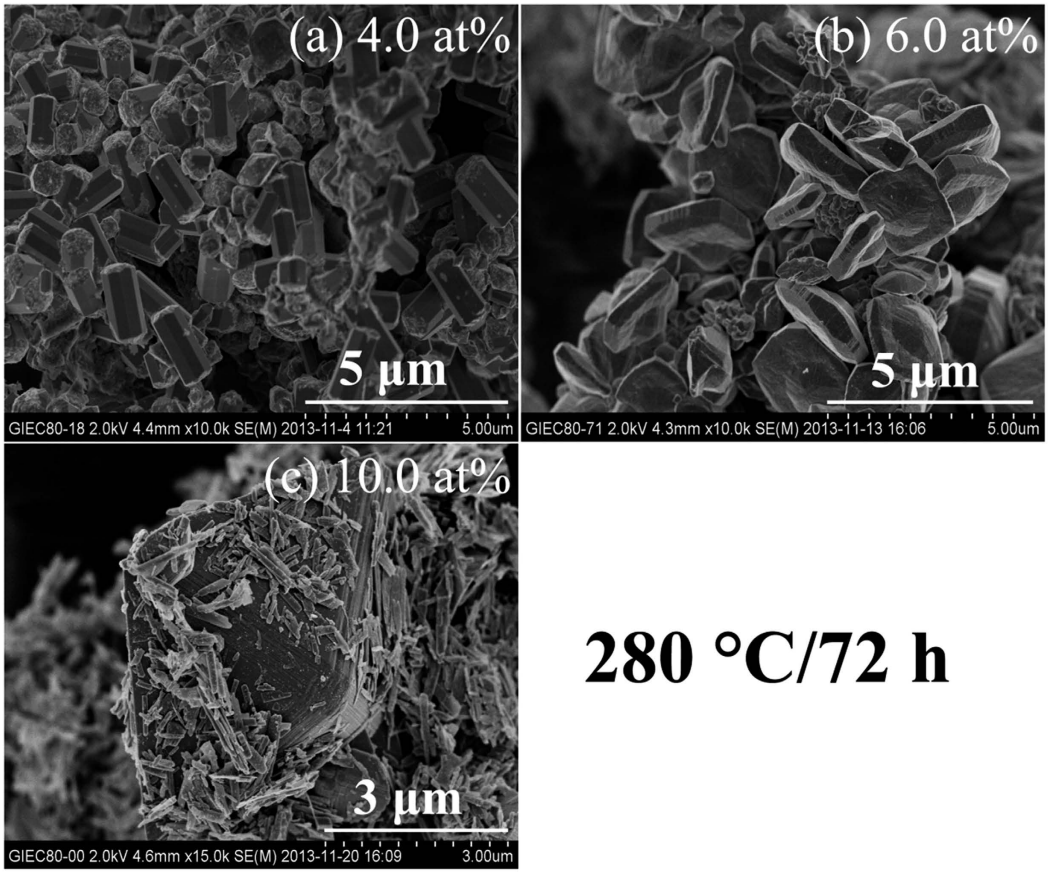

Figure 8. SEM images of the $W_xV_{1-x}O_2$ prepared at 280 °C for 72 h with different W doping levels. (**a**) 4.0 at.% (**b**) 6.0 at.% (**c**) 10.0 at.%.

$W_xV_{1-x}O_2$ with x = 4.0, 6.0 and 10.0 at% were prepared at 280 °C for 72 h to investigate more W dopant on the crystalline phase metamorphic and morphology transition behavior of the as-obtained products as shown in Figs 7 and 8. Pure phase VO_2(R) is still obtained for the 4.0 and 6.0 at% sample. When the W-doped level increases to 10.0 at%, VO_2(B) nanobelts are grown again besides the main phase VO_2(R). The results indicate a certain doping level of W could promote VO_2(B) metamorphoses to pure phase VO_2(M/R), which agrees with the previous reports[14,18]. Whereas, more excess W dopant would prevent the metamorphosis from VO_2(B) into VO_2(R) thoroughly. The intensity ratio between the XRD peaks of {110} and that of {101} of VO_2(R) prepared at 280 °C for 72 h with different W-doped levels

W-doped level (at. %)	Intensity ratio {110}/{101}
1.0	2.1
2.0	5.7
4.0	2.5
6.0	1.9
10.0	1.1

Table 1. Intensity ratio between the XRD peaks of {110} and that of {101} of $W_xV_{1-x}O_2$ prepared at 280 °C for 72 h with different W-doped levels.

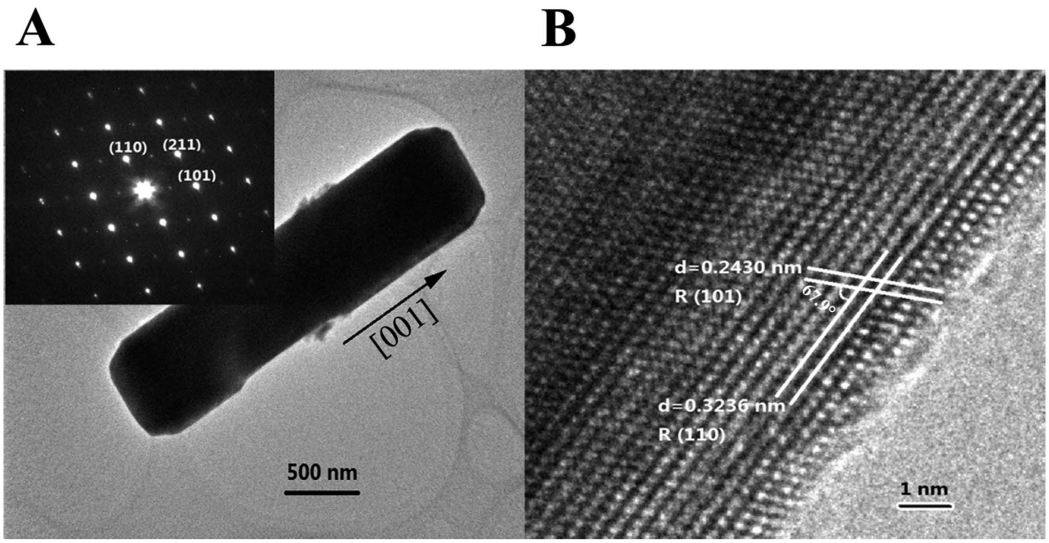

Figure 9. (**A**) TEM image of the single VO_2 nanorod for the W-doped 4.0 at% sample and the corresponding SAED pattern (inset). (**B**) Lattice-resolved HRTEM image of the single nanorod.

is listed in Table 1. It increases significantly from 2.1 to 5.7 with increasing the W-doped level from 1.0 to 2.0 at%. The strong intensity of the {110} reflections points to the strongly preferential growth direction of the structures, as has also been noted previously for VO_2 nanowires prepared at high temperatures by vapor transport[31–33]. Simultaneously, the aspect ratio of the VO_2(R) nanorods increases from nearly 5 to 10 with the increased dopant. Whereas, if the W-doped level increases from 4.0 to 10.0 at%, the intensity ratio {110}/{101} decreases from 2.5 to 1.1. Meanwhile, the aspect ratio of nanorods decreases with the increased W dopant as shown in Fig. 8. Finally, the bulk crystal of VO_2(R) is grown for the 10.0 at% sample. The results indicate a certain doping level of W can promote the preferential growth of R {110} and the increased aspect ratio of VO_2(R) nanorods, whereas the excess W would restrain.

The shape-controlled mechanism revealed by TEM. The length of W-doped 4.0 at% VO_2 nanorods (synthesized at 280 °C for 72 h) is about 2.5 μm with 600 nm in diameter as shown in the low magnification TEM image in Fig. 9A. The single-crystalline nanorods is confirmed by the lattice images of HRTEM and the inset SAED pattern as shown in Fig. 9. The lattice constants observed in Fig. 9B are 0.3236 and 0.2430 nm respectively, which can be indexed to the spacing of R {110} and R {101}, and the angle between the two lattice images is 67.9° in arc and this corresponds to the angle between the designated crystal planes of R (110) and R (101). In addition, the (001) plane orientation is just perpendicular to the nanorod' growth direction R (110), and revealing the preferential growth direction of the VO_2(R) nanorods is along [001]. The results demonstrate that the preferential growth of nanorod' growth direction R (110) is responsible for the increased aspect ratio of VO_2(R) nanorods. It is generally known that the greater the d-spacing, the atom arrange more closely on the crystal plane. For the body-centered tetragonal VO_2(R), (110) with the largest d-spacing contributes to the lowest surface energy for the preferential growth of VO_2 grains. According to the SAED pattern shown in the inset of Fig. 9A, the bright diffraction spots reveal the good crystallinity of the sample. Based on the Bragg equation, the diffraction spots can be ascribed to different crystal planes of VO_2(R). The three Bravais lattice points shown in the SAED of the inset of Fig. 9A correspond to crystal planes of R (110), R (101) and R (211) respectively as indexed therein. This definitely demonstrates the nanorods belong to VO_2(R). Moreover, no fringe

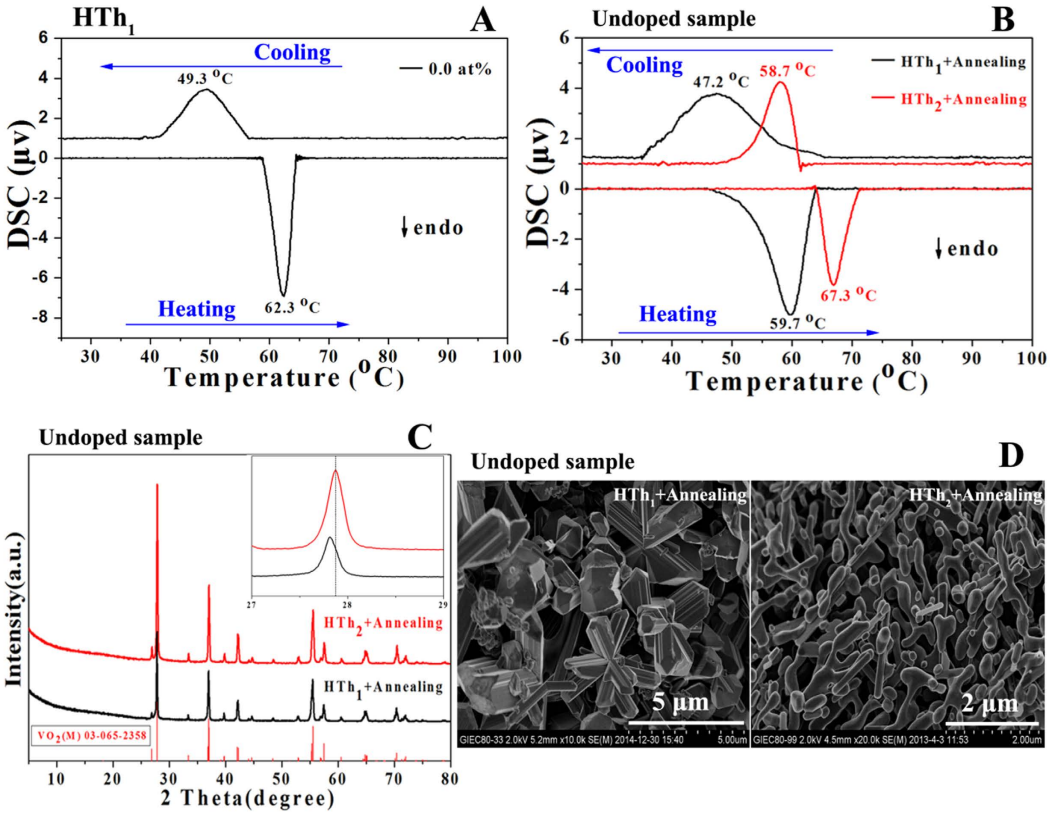

Figure 10. (**A**) DSC curve of the hydrothermal sample treated at 280 °C for 72 h (HTh_1) with W-doped at 0.0 at%. (**B**) DSC curves for the undoped samples synthesized by the (HTh_1 + Annealing) (annealing at 500 °C for 1 h in furnace) method and the (HTh_2 + Annealing) (hydrothermal treated at 160 °C for 72 h) process respectively. (**C**) XRD patterns of the undoped samples synthesized by the designated two fabrication processes. The red column belongs to standard pattern in JCPDS card No. 65–2358 for VO_2(M). (**D**) SEM images of the undoped samples synthesized by the designated two fabrication processes.

spacing belongs to tungsten oxides or their derivatives are detected by HRTEM, which confirms the capture of W atoms into the crystal lattice of VO_2 as mother matrix and the formation of homogeneous solid-solution of $W_xV_{1-x}O_2$.

Influence of oxygen nonstoichiometry on the phase transition behavior. Figure 10A shows the DSC curve of the hydrothermally undoped sample treated at 280 °C for 72 h (HTh_1). The endothermic and exothermal transition temperature is 62.3 and 49.3 °C during heating and cooling cycles respectively. Thus, the phase transition temperature (defined as $T_c = (T_{c,h} + T_{c,c})/2$) of the undoped micron-sized block and snowflake-like sample is about 55.8 °C, which is much lower than the transition temperature of undoped bulk VO_2 (about 68 °C) reported by Morin[4] and undoped nanobelts VO_2 (64 °C) reported by Whittaker[24]. The hysteresis width ($\triangle T = T_{c,h} - T_{c,c}$) of the undoped sample is about 13.0 °C.

To study the unusual low T_c for the HTh_1 synthesized undoped sample, we directly compare the DSC for this sample by the after annealing (HTh_1 + Annealing) with that for the hydrothermal undoped one treated at 160 °C for 72 h and after annealing (HTh_2 + Annealing) (annealing at 500 °C for 1 h in high-purity argon and this being also prepared by our group[34]) as shown in Fig. 10B. For the sake of comparison, we list Table 2 to show T_c and hysteresis width depending on the W-doped level and fabrication processes. When the undoped sample is synthesized by the (HTh_1 + Annealing) process, $T_{c,h}$ and $T_{c,c}$ is about 59.7 and 47.2 °C respectively. Therefore, the T_c is about 53.5 °C, which is also lower than the (HTh_2 + Annealing) fabricated undoped one (T_c being c.a 63.0 °C as shown in Table 2). Figure 10C shows the XRD patterns of the undoped samples synthesized by the designated two fabrication processes. The peaks of VO_2(B) vanish and all of the peaks can be indexed to pure phase VO_2(M) for the HTh_1 synthesized undoped sample by the after annealing, which is similar to the (HTh_2 + Annealing) fabricated one. The inset close-up shows that M (011) peak shifts to low angles when comparing the (HTh_1 + Annealing) synthesized undoped sample with those by the (HTh_2 + Annealing) synthesized one, which indicates the lattice spacing of M (011) increases. Both micron-sized snowflake and block-like morphologies are observed for the (HTh_1 + Annealing)

Sample	Phase transition temperature		Hysterisis width △T	T_c
	Heating cycle $T_{c,h}$	Cooling cycle $T_{c,c}$		
HTh_1 undoped $VO_{1.96}$	62.3 °C	49.3 °C	13.0 °C	55.8 °C
HTh_1 + Annealing undoped $VO_{1.95}$	59.7 °C	47.2 °C	12.5 °C	53.5 °C
HTh_2 + Annealing undoped $VO_{2.00}$	67.3 °C	58.7 °C	8.6 °C	63.0 °C

Table 2. DSC parameters of the HTh_1 synthesized sample with W-doped at 0.0 at% and of the undoped samples synthesized by the (HTh_1 + Annealing) method and the (HTh_2 + Annealing) process respectively.

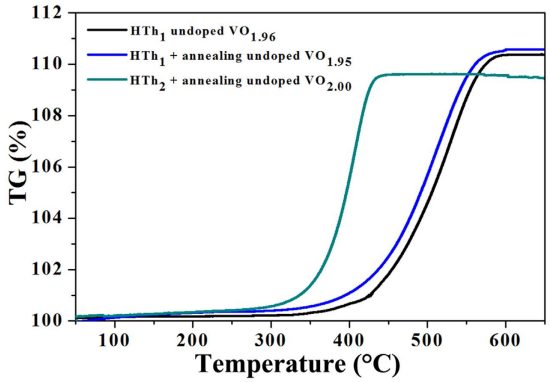

Figure 11. The thermogravimetric analysis of the samples.

synthesized undoped sample as shown in Fig. 10D. Whereas, nanostructure is grown by the (HTh_2 + Annealing) fabrication process. Thanks to the formation energies of oxygen vacancies in rutile oxides are very high, the high hydrothermal temperature (280 °C) and reductive hydrothermal atmosphere for the (HTh_1 + Annealing) method may contribute to the generation of oxygen vacancies to form non-stoichiometric $VO_{2-\delta}$ compared to the (HTh_2 + Annealing) process (160 °C), and this would promote the lattice structural transition[35,36].

Discussion. To determine the oxygen stoichiometry, the thermogravimetric analysis of the samples was conducted as shown in Fig. 11. According to the TG curves, it can be found there exists one stage for the complete oxidization of the samples in the range of 300–600 °C. The weight gain (Δ_{TG}) is about 10.4 %, 10.5 % and 9.6 % for the HTh_1 synthesized undoped VO_x, (HTh_1 + annealing) undoped VO_y and (HTh_2 + annealing) undoped VO_z respectively. The reaction equations for the oxidization of the samples can be given as follows (1):

$$VO_x + \frac{2.5-x}{2}O_2 \xrightarrow{\Delta} VO_{2.5} \quad (1)$$

$$\text{Thus, } \Delta_{TG} = (2.5 - x) \times M_O/M_{VOx} \quad (2)$$

Where M_O and M_{VOx} represent molar mass of oxygen and VO_x respectively. When combining the above formulas (2) and experimental results, we can work out x = 1.96, y = 1.95 and z = 2.00 respectively. The fact demonstrates that oxygen deficiency is formed in the HTh_1 synthesized undoped $VO_{1.96}$ and (HTh_1 + annealing) undoped $VO_{1.95}$, and the precisely stoichiometric $VO_{2.00}$ is formed in the (HTh_2 + annealing) undoped sample. Son and co-workers have synthesized monoclinic VO_2 micro- and nanocrystals by optimizing the hydrothermal conditions[37]. In their research, the phase transition temperature of stoichiometric $VO_{2.00}$ microrods is around 68 °C. Usually, the T_c of MIT for VO_2 is affected by doping, nanoscaling, nonstoichiometry, strain and etc[12,30,38,39]. For the HTh_1 synthesized undoped micron-sized $VO_{1.96}$, the reason for the unusual low T_c may be due to the oxygen nonstoichiometry. The nano-size effect may be responsible for the relative lower T_c (63 °C) of the (HTh_2 + Annealing) synthesized stoichiometric $VO_{2.00}$ nanostructure.

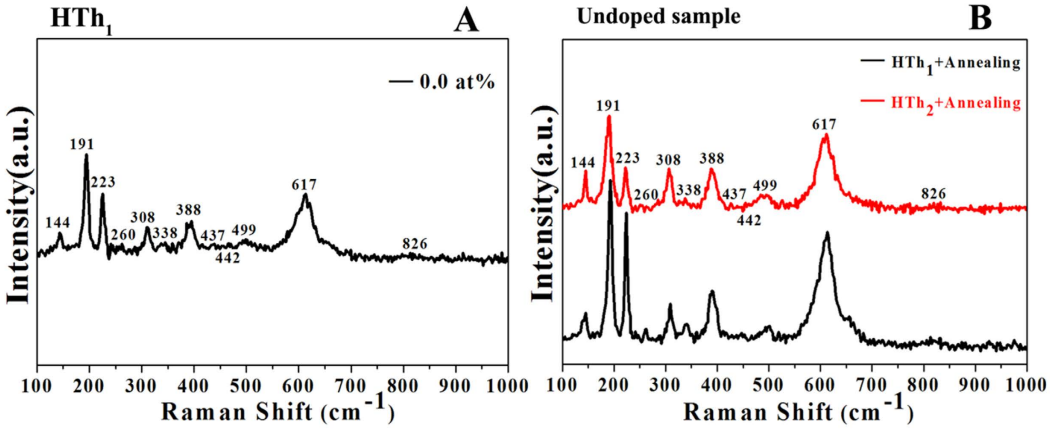

Sample	Intensity ratio 191/223
HTh_1 undoped $VO_{1.96}$	1.6
HTh_1+Annealing undoped $VO_{1.95}$	1.3
HTh_2+Annealing undoped $VO_{2.00}$	2.3

Figure 12. (**A**) Raman spectra of the HTh_1 synthesized sample with W-doped at 0.0 at% in the Raman shift range 100–1000 cm^{-1}. (**B**) Raman curves for the undoped samples synthesized by the (HTh_1 + Annealing) method and the (HTh_2 + Annealing) process respectively.

Figure 12A,B shows the Raman spectra of the samples depending on dopant level and fabrication processes. The peaks in the Raman spectra are all identified as 144 (B_{1g}), 191 (A_g), 223 (A_g), 260 (A_g), 308 (A_g), 338 (A_g), 388 (A_g), 437 (A_g), 442 (E_g), 499 (A_g), 617 (A_{1g}), and 826 (B_{2g}) cm^{-1} respectively, and these Raman-active modes are the clear evidence of the existing of VO_2(M) belonging to space group C^5_{2h}, which agrees with the identified Raman peaks by other researchers[40–43]. The intensity ratio between the peak of 191 and that of 223 cm^{-1} (191/223) of the HTh_1 synthesized undoped $VO_{1.96}$ is 1.6. When comparing the (HTh_2 + Annealing) synthesized undoped $VO_{2.00}$ with those by the (HTh_1 + Annealing) synthesized undoped $VO_{1.95}$, the intensity ratio decreases from 2.3 to 1.3. H. T. Kim and co-workers have studied Raman spectra for the MIT of the undoped VO_2 in detail and deduced the conclusion that the Raman-active A_g modes at 191 and 223 cm^{-1} were explained by the pairing and the tilting of V cations respectively[43]. Hence, the decreased relative intensity of 191 cm^{-1} peak suggests the depairing of V cations and the occurring of the localized structural phase transition (SPT, induced possibly by oxygen nonstoichiometry for the HTh_1 synthesized undoped $VO_{1.96}$ and (HTh_1 + annealing) undoped $VO_{1.95}$), and this might cause the transformation from the intrinsic structure of the matrix of VO_2(M) to the localized rutile structure. In addition, the local rutile structure is the structure-guided domain, which will act as the initial nucleation site for the whole SPT[44]. This process might promote MIT for the origin of the lowering T_c. However, this origin is still under the debate among the concerned experts as cited in the literature by Y. Xie *et al.* for an example, who pointed out that the atomic structure of isolated W dopant play a role in driving the nearby symmetric monoclinic VO_2 lattice towards rutile phase, resulting in the depression of T_c[45,46]. Hence the exact mechanism for the observed unusual phenomena requires our further investigation.

Conclusions

In this study, pure phase VO_2(M/R) with controlled morphology were successfully prepared via one-step hydrothermal method. The addition of a certain level of W (0.5–2.0 at%) is vital to synthesize the pure phase VO_2(M/R) nanorods. The assured level of W doping can promote the preferential growth of {110} to form VO_2(M/R) nanorods with high aspect ratio. It must be emphasized that the unusual low T_c equals to 55.8 and 53.5 °C is observed for the nonstoichiometric $VO_{1.96}$ and $VO_{1.95}$ in the bulk respectively, and the T_c is 63.0 °C for the precisely stoichiometric $VO_{2.00}$ nanostructure. The present study demonstrates an improvement of the phase transition behavior and reduces the hindrances for the advanced applications of VO_2-based materials.

Methods

Materials. Oxalic acid ($H_2C_2O_4{\cdot}2H_2O$, AR) and vanadium pentoxide (V_2O_5, AR) were used as source material to prepare the vanadium precursor solution. Deionized water ($\rho = 18.2\,M\Omega.cm$) was used to prepare all aqueous solutions. Ammonium tungstate hydrate ($(NH_4)_5H_5[H_2(WO_4)_6]{\cdot}H_2O$, AR) was chosen as the W dopant. All of these reagents were used without further purification.

The preparation process. The detail of this part has been described in previous report[30]. Briefly, V_2O_5 and oxalic acid (1: (1–3) in molar ratio) were directly added to 75 ml deionized water at RT. Then, a certain amount of W dopant was dispersed into the above solution with magnetic stirring. After mixing for 1 h, the resulting precursor was transferred into a 100 mL stainless steel autoclave with polyphenylene cup, then being sealed and maintained at 280 °C for 6–72 h. After the autoclave cooling to RT, a dark blue precipitate was obtained. The product was washed with deionized water and acetone for several times, then centrifuged at 8000 rpm for 8 min and dried in vacuum at 60 °C for 6 h.

In this study, $(NH_4)_5H_5[H_2(WO_4)_6]{\cdot}H_2O$ was used as the W dopant, and the reported W-doped content here is based on the quantity of W atoms added in the feed. The sample synthesized by the duration of the hydrothermal time for 6 or 72 h is simplified to the 6 or 72 h-sample.

Characterization techniques. The phase purity of the products was examined by an X-ray diffractometer (XRD, PANalytical X'pert Pro MPD) in the 2θ range of 5–80° with the step of 0.0083° using Cu-Kα radiation ($\lambda = 1.54178$ Å). The operating voltage and current were kept at 40 kV and 40 mA, respectively. The morphology and dimensions of the products were investigated using a field emission scanning electron microscope (FESEM, S-4800, Hitachi Japan) under the operating voltage of 2 kV. A JEOL-2100F instrument operated at 200 kV was used to acquire high-resolution transmission-electron-microscopy (HRTEM) images and selected area electron diffraction (SAED) patterns. Raman scattering spectra of the samples were recorded on a LabRAM HR800 micro-Raman spectrometer using a 532 nm wavelength YAG laser. The phase transition properties depending on the surrounding temperature of the as-prepared VO_2 were studied by differential scanning calorimetry (HDSC, PT500LT/1600) under the temperature range from 25 to 100 °C under the circulatory heating/cooling cycles. The thermogravimetric analysis (TG) of the samples was conducted on a Nicolet 6700-Q50 thermal analyzer under dry air flow in the range of 50–650 °C with a heating rate of 5 °C min^{-1}.

References

1. Wu, C. Z. *et al.* Direct hydrothermal synthesis of monoclinic VO_2(M) single-domain nanorods on large scale displaying magnetocaloric effect. *J. Mater. Chem.* **21,** 4509–4517 (2011).
2. Hormoz, S. & Ramanathan, S. Limits on vanadium oxide Mott metal–insulator transition field-effect transistors. *Solid State Electronic* **54,** 654–659 (2010).
3. Chen, Z. *et al.* VO_2-based double-layered films for smart windows: Optical design, all-solution preparation and improved properties. *Sol. Energy Mater. Sol. Cells*. **95,** 2677–2684 (2011).
4. Morin, F. J. Oxides which show a metal-to-insulator transition at the Neel temperature. *Phys. Rev. Lett.* **3,** 34–36 (1959).
5. Netsianda, M., Ngoepe, P. E., Catlow, C. R. A. & Woodley, S. M. The Displacive Phase Transition of Vanadium Dioxide and the Effect of Doping with Tungsten. *Chem. Mater.* **20,** 1764–1772 (2008).
6. Andersson, G. Studies on vanadium oxides. *Acta Chem. Scand.* **8,** 1599–1606 (1954).
7. Corr, S. A. *et al.* Controlled reduction of vanadium oxide nanoscrolls: crystal structure, morphology, and electrical properties. *Chem. Mater.* **20,** 6396–6404 (2008).
8. Kim, H. K. *et al.* Finite-size effect on the first-order metal-insulator transition in VO_2 films grown by metal-organic chemical-vapor deposition. *Phys. Rev. B* **47,** 12900–12907 (1993).
9. Alivisatos, A. P. Semiconductor Clusters, Nanocrystals, and Quantum Dots. *Science* **271,** 933–937 (1996).
10. Odom, T. W., Huang, J. L., Kim, P. & Lieber, C. M. Structure and electronic properties of carbon nanotubes. *J. Phys. Chem. B* **104,** 2794–2809 (2000).
11. Liu, X. *et al.* Structure and magnetization of small monodisperse platinum clusters. *Phys. Rev. Lett.* **97,** 253401-1–253401-4 (2006).
12. Whittaker, L., Jaye, C., Fu, Z., Fischer, D. A. & Banerjee, S. Depressed phase transition in solution-grown VO_2 nanostructures. *J. Am. Chem. Soc.* **131,** 8884–8894 (2009).
13. Dai, L., Cao, C. X., Gao, Y. F. & Luo, H. J. Synthesis and phase transition behavior of undoped VO_2 with a strong nano-size effect. *Sol. Energy Mater. Sol. Cells* **95,** 712–715 (2011).
14. Katzke, H., Toledano, P. & Depmeier, W. Theory of morphotropic transformations in vanadium oxides. *Phys. Rev. B* **68,** 024109-1–024109-7 (2003).
15. Popuri, S. R. *et al.* Rapid hydrothermal synthesis of VO_2(B) and its conversion to thermochromic $VO_2(M_1)$. *Inorg. Chem.* **52,** 4780–4785 (2013).
16. Zhang, K. F., Liu, X., Su, Z. X. & Li, H. L. VO_2(R) nanobelts resulting from the irreversible transformation of VO_2(B) nanobelts. *Mater. Lett.* **61,** 2644–2647 (2007).
17. Kam, K. C. & Cheetham, A. K. Thermochromic VO_2 nanorods and other vanadium oxides nanostructures. *Mater. Res. Bull.* **41,** 1015–1021 (2006).
18. Li, J., Liu, C. Y. & Mao, L. J. The character of W-doped one-dimensional VO_2(M). *J. Solid State Chem.* **182,** 2835–2839 (2009).
19. Qazilbash, M. M. *et al.* Mott transition in VO_2 revealed by infrared spectroscopy and nano-imaging. *Science* **318,** 1750–1753 (2007).
20. Kim, H. T. *et al.* Monoclinic and correlated metal phase in VO_2 as evidence of the Mott transition: coherent phonon analysis. *Phys. Rev. Lett.* **97,** 266401-1–266401-4 (2006).
21. Booth, J. M. & Casey, P. S. Anisotropic Structure Deformation in the VO_2 Metal-Insulator Transition. *Phys. Rev. Lett.* **103,** 086402-1–086402-4 (2009).
22. Goodenough, J. B. The two components of the crystallographic transition in VO_2. *J. Solid State Chem.* **3,** 490–500 (1971).

23. Haverkort, M. W. *et al.* Orbital-Assisted Metal-Insulator Transition in VO_2. *Phys. Rev. Lett.* **95,** 196404-1–196404-4 (2005).
24. Whittaker, L., Wu, T. L., Patridge, C. J., Sambandamurthy, G. & Banerjee, S. Distinctive finite size effects on the phase diagram and metal–insulator transitions of tungsten-doped vanadium (iv) oxide. *J. Mater. Chem.* **21,** 5580–5592 (2011).
25. Hörlin, T., Niklewski, T. & Nygren, M. Electrical and magnetic properties of $V_{1-x}W_xO_2$, $0 \leq x \leq 0.060$. *Mater. Res. Bull.* **7,** 1515–1524 (1972).
26. Reyes, J. M., Sayer, M. & Chen, R. Transport properties of tungsten-doped VO_2. *Can. J. Phys.* **54,** 408–412 (1976).
27. Zhang, Y. F. *et al.* Direct preparation and formation mechanism of belt-like doped VO_2(M) with rectangular cross sections by one-step hydrothermal route and their phase transition and optical switching properties. *J. Alloys Comp.* **570,** 104–113 (2013).
28. Nazari, M., Chen, C., Bernussi, A. A., Fan, Z. Y. & Holtz, M. Effect of free-carrier concentration on the phase transition and vibrational properties of VO_2. *Appl. Phys. Lett.* **99,** 071902-1–071902-3 (2011).
29. Liu, H. W., Wong, L. M., Wang, S. J., Tang, S. H. & Zhang, X. H. Effect of oxygen stoichiometry on the insulator-metal phase transition in vanadium oxide thin films studied using optical pump-terahertz probe spectroscopy. *Appl. Phys. Lett.* **103,** 151908-1–151908-5 (2013).
30. Chen, R. *et al.* One-step hydrothermal synthesis of $V_{1-x}W_xO_2$(M/R) nanorods with superior doping efficiency and thermochromic properties. *J. Mater. Chem. A* **3,** 3726–3738 (2015).
31. Guiton, B. S., Gu, Q., Prieto, A. L., Gudiksen, M. S. & Park, H. Single-crystalline vanadium dioxide nanowires with rectangular cross sections. *J. Am. Chem. Soc.* **127,** 498–499 (2005).
32. Beteille, F., Morineau, R., Livage, J. & Nagano, M. Switching properties of $V_{1-x}Ti_xO_2$ thin films deposited from alkoxides. *Mater. Res. Bull.* **32,** 1109–1117 (1997).
33. Binions, R., Hyett, G., Piccirillo, C. & Parkin, I. P. Doped and un-doped vanadium dioxide thin films prepared by atmospheric pressure chemical vapour deposition from vanadyl acetylacetonate and tungsten hexachloride: the effects of thickness and crystallographic orientation on thermochromic properties. *J. Mater. Chem.* **17,** 4652–4660 (2007).
34. Xiao, X. D. *et al.* A facile process to prepare one dimension VO_2 nanostructures with superior metal-semiconductor transition. *CrystEngComm* **15,** 1095–1106 (2013).
35. O'Brien, A., Woodward, D. I., Sardar, K., Walton, R. I. & Thomas, P. A. Inference of oxygen vacancies in hydrothermal $Na_{0.5}Bi_{0.5}TiO_3$. *Appl. Phys. Lett.* **101,** 142902-1–142902-4 (2012).
36. Jeong, J. *et al.* Suppression of metal-insulator transition in VO_2 by electric field–induced oxygen vacancy formation. *Science* **339,** 1402–1405 (2013).
37. Son, J. H., Wei, J., Cobden, D., Cao, G. Z. & Xia, Y. N. Hydrothermal Synthesis of Monoclinic VO_2 Micro- and Nanocrystals in One Step and Their Use in Fabricating Inverse Opals. *Chem. Mater.* **22,** 3043–3050 (2010).
38. Griffiths, C. H. & Eastwood, H. K. Influence of stoichiometry on the metal-semiconductor transition in vanadium dioxide. *J. Appl. Phys.* **45,** 2201–2206 (1974).
39. Ruzmetov, D., Senanayake, S. D., Narayanamurti, V. & Ramanathan, S. Correlation between metal-insulator transition characteristics and electronic structure changes in vanadium oxide thin films. *Phys. Rev. B* **77,** 195442-1–195442-5 (2008).
40. Wu, J. M. & Liou, L. B. Room temperature photo-induced phase transitions of VO_2 nanodevices. *J. Mater. Chem.* **21,** 5499–5504 (2011).
41. Chen, C., Wang, R., Shang, L. & Guo, C. Gate-field-induced phase transitions in VO_2: monoclinic metal phase separation and switchable infrared reflections. *Appl. Phys. Lett.* **93,** 171101-1–171101-3 (2008).
42. Schilbe, P. Raman scattering in VO_2. *Physica B* **316,** 600–602 (2002).
43. Kim, H. T. *et al.* Raman study of electric-field-induced first-order metal-insulator transition in VO_2-based devices. *Appl. Phys. Lett.* **86,** 242101-1–242101-3 (2005).
44. Wu, Y. F. *et al.* Depressed transition temperature of $W_xV_{1-x}O_2$: mechanistic insights from the X-ray absorption fine structure (XAFS) spectroscopy. *Phys. Chem. Chem. Phys.* **16,** 17705–17714 (2014).
45. Yao, T. *et al.* Understanding the Nature of the Kinetic Process in a VO_2 Metal-Insulator Transition. *Phys. Rev. Lett.* **105,** 226405-1–226405-4 (2010).
46. Tan, X. G. *et al.* Unraveling Metal-insulator Transition Mechanism of VO_2 Triggered by Tungsten Doping. *Sci. Rep.* **2,** 466, doi: 10.1038/srep00466 (2012).

Acknowledgements

This work was supported by Science and Technology Planning Project of Guangdong Province, China (Grant No. 2013B050800006), External Cooperation Program of BIC, Chinese Academy of Sciences (Grant No. 182344KYSB20130006).

Author Contributions

M.L. proposed and organized the overall project. C.R. performed the sample synthesis, TEM and phase transition behavior analysis. C.R. prepared the manuscript with discussion from M.L., L.C.Y., Z.J.H., C.H.L. and T.S., A.T. and I.Y. accomplished TEM sample preparation and observation. All the authors discussed the results.

Additional Information

Competing financial interests: The authors declare no competing financial interests.

How to cite this article: Chen, R. *et al.* Shape-controlled synthesis and influence of W doping and oxygen nonstoichiometry on the phase transition of VO_2. *Sci. Rep.* **5**, 14087; doi: 10.1038/srep14087 (2015).